Effect of grain boundary structures on the behavior of He defects in Ni: An atomistic study*

H F Gong(龚恒风)[1,2,3,4,†], Y Yan(严岩)[1], X S Zhang(张显生)[1], W Lv(吕伟)[4], T Liu(刘彤)[1], and Q S Ren(任啟森)[1]

[1] *ATF R&D, China Nuclear Power Technology Research Institute Co., Ltd, Shenzhen* 518000, *China*
[2] *Shanghai Institute of Applied Physics, Division of Nuclear Materials and Engineering, Chinese Academy of Sciences, Shanghai* 201800, *China*
[3] *Key Laboratory of Interfacial Physics and Technology, Chinese Academy of Sciences, Shanghai* 201800, *China*
[4] *Department of Mechanical Engineering, University of Michigan, Ann Arbor, Michigan* 48109, *USA*

(Received 23 March 2017; revised manuscript received 23 May 2017; published online 18 July 2017)

We investigated the effect of grain boundary structures on the trapping strength of He_N (N is the number of helium atoms) defects in the grain boundaries of nickel. The results suggest that the binding energy of an interstitial helium atom to the grain boundary plane is the strongest among all sites around the plane. The He_N defect is much more stable in nickel bulk than in the grain boundary plane. Besides, the binding energy of an interstitial helium atom to a vacancy is stronger than that to a grain boundary plane. The binding strength between the grain boundary and the He_N defect increases with the defect size. Moreover, the binding strength of the He_N defect to the $\Sigma3(1\bar{1}2)[110]$ grain boundary becomes much weaker than that to other grain boundaries as the defect size increases.

Keywords: molecular dynamics, trapping strength, helium defect, grain boundary

PACS: 31.15.at, 33.15.Fm, 31.15.es, 31.30.jf **DOI:** 10.1088/1674-1056/26/9/093104

1. Introduction

The interaction of helium (He) defects with the grain boundary (GB) is of fundamental importance for the generation-IV molten salt reactor (MSR), where the structural materials of Ni-based alloys are exposed to the harsh reactor environment with high-temperature, strong corrosion, and high flux of He by the (n, α) transmutation reactions. Due to their extremely low solubility, He defects have a strong tendency to be trapped in other defect regions containing an excess volume, such as vacancies, dislocations, and GBs. This process leads to the subsequent formation of He bubbles (or voids) within those defects.[1–4] The formation of He bubbles in a material can lead to void swelling, high temperature intergranular embrittlement, surface roughening, blistering, etc., which will significantly degrade the mechanical properties of the material and negatively impact the lifetime and safety of a reactor.[5–8]

Previous experimental studies have attributed He embrittlement to the clustering and migration of He bubbles toward microscale features, such as GBs and dislocations.[9–11] He bubbles have been proposed to cause, for example, the initiation of GB cracks and premature brittle failure of materials together with a drastic reduction in ductility under static and cyclic loads.[12] Although microstructural changes caused by grain boundary bubble formation can be observed with several experimental techniques such as transmission electron microscopy (TEM) and small-angle neutron scattering (SANS), these techniques cannot directly observe He segregation at GBs without bubble formation. Studies have used TEM and He thermal desorption spectrometry (TDS) to investigate the effect of alloying elements on the mechanism of bubble growth and migration.[13] To test the hypothesis that the surface of nanoclusters is a preferential nucleation site for He bubbles, Edmonson *et al.*[14] studied a nanostructured ferritic alloy irradiated with He^+ ions. The results showed He bubble nucleation on the surface of nanoclusters and Ti (N, C) precipitates along GBs and dislocations. However, how the He bubble interacts with defects, especially at GBs, remains unclear. In addition, advances in experiment technology and theoretical method may motivate new thinking. For instance, the interstitial He diffusion along GBs was considered to be slower than He diffusion in grains,[15] while recent thermal He desorption experiments indicated that GBs may act as easy paths for He diffusion toward surfaces.[16]

To date, there have been several studies using first principles and molecular dynamics (MD) simulations to investigate how He bubbles segregate at GBs in metals.[17–21] There have been relatively few studies focusing on He interaction with GBs.[22–29] MD simulations have been used to understand the migration of interstitial He inside different GBs[30] and to understand how the GB strength is affected by He or He bubbles.[31–33] First principles calculations have

*Project supported by the Program of International S&T Cooperation, China (Grant No. 2014DFG60230), the National Basic Research Program of China (Grant No. 2010CB934504), Strategically Leading Program of the Chinese Academy of Sciences (Grant No. XDA02040100), the Shanghai Municipal Science and Technology Commission, China (Grant No. 13ZR1448000), the National Natural Science Foundation of China (Grant Nos. 91326105 and 21306220).

†Corresponding author. E-mail: gonghengfeng@cgnpc.com.cn

© 2017 Chinese Physical Society and IOP Publishing Ltd

been used to understand the diffusion and stability of He defects at the Σ5(310) symmetric tilt GB (STGB).[34] Kurtz and Heinisch applied the Finnis–Sinclair potential in MD simulations, showing that substitutional He is more weakly bound to the GB plane than the interstitial He.[22] Gao *et al.*[23] investigated the relationship between the maximum binding energy and the GB. Hammond *et al.*[35] showed that the GB does not facilitate He transport in tungsten and several other metals. Kashinath *et al.*[36] showed that nanoscale platelets at semi-coherent interfaces can store He bubbles, and these bubbles can remain stable under irradiation. However, there are a number of unresolved issues related to how the He defect interacts with GBs, especially in Ni-based alloys. For example, existing studies using atomistic simulations have not considered a wide range of GB structures to understand the effects of macroscopic variables on the binding properties of the N-th He atom to the remaining $He_{N-1}V_M$ defect (N is the number of He atoms and M is the number of vacancies), especially the behavior of He defects in the GB of Ni, or the interaction between the He_NV_M defect and the GB. Establishing a trend of these binding properties for Ni-based alloys will be very useful for mesoscale simulations of He bubble nucleation and growth.

This paper focuses on understanding how the GB of Ni interacts with the interstitial He atom, its dependence on the distance of the He defect from the center of the GB plane, and how the local atomistic environment in GBs affects the trapping strength of the N-th He atom to the remaining He_{N-1} defect, as well as the trapping strength of the He_NV_M defect to the GB in Ni-based alloys. The outline of the paper is as follows. The computational techniques are presented in Section 2. In Section 3, we calculate the interaction between five STGBs and He_N defects. Section 4 presents the conclusion.

2. Methodology

All calculations were performed using MD simulations with the LAMMPS software package.[37] In the simulation cell, the atomic interactions of Ni–Ni, Ni–He, and HeHe–He atoms were described by the modified analytic embedded atom method (MAEAM),[38–47] the Morse potential,[48] and the Lennard–Jones potential,[49] respectively. More information about the formulas and parameters can be found in Ref. [29]. In our MD simulations, the conjugate gradient (CG) algorithm and the Nosé constant-temperature technique[50] with a time step of 0.5 fs were used. Due to different GB configurations, the total simulation time varied between 100.0 ps and 150.0 ps. Firstly, the initial configurations of GB were constructed by the GB studio software package,[51] as shown in Fig. 1. The output of the GB studio calculations served as the input of the MD simulation. However, before being written into MD simulation, the GB needed to go through a relax and quench phase in order to obtain the truly stable GB structure. Secondly, an interstitial He atom was placed initially into the GB, and energy minimization was performed for the simulation cell by iteratively adjusting the atomic coordinates with a conjugate gradient algorithm so that high overlapping atoms could adjust their positions. Thirdly, Ni atoms were equilibrated at 300 K for 25 ps using NVT ensemble for the system to relax to an equilibrium state. Finally, the simulation cell was quenched to 0 K to obtain the stable GB configuration with an interstitial He atom. The same quench process was employed to obtain other stable GB configurations with each additional He atom. When a He atom was added to around the GB plane, it was inserted into a spherical region centered at the GB plane with a radius of 1.0 Å. Starting from the GB plane, the He atom was inserted every 1 Å perpendicular to the GB plane at each time in order to study the relationship between the distance and the binding energy. Besides, He_N defects in the GB planes were formed by inserting He atoms into the sphere of 1.0 Å radius around the GB plane accordingly each time. The same procedures of energy minimization, relax, and quench were carried out as previously to obtain the final stable GB structures containing He defects. In the simulation procedure, He interstitials were frozen, avoiding the He atom diffusion. An interstitial He atom was inserted into the GB to calculate the trapping strength of the GB to the He defect.

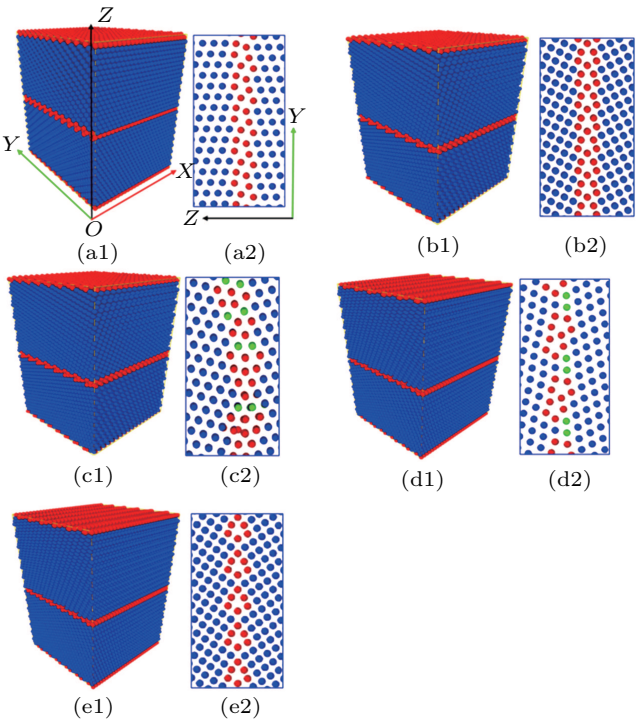


Fig. 1. (color online) Atomic blocks showing the initial and final stable STGBs analyzed using the common neighbor analysis (CNA). The blue balls represent the FCC crystal structure. The red balls represent the irregular crystal structures. The green balls represent the HCP crystal structure. (a) Σ3 GB; (b) Σ5 GB; (c) Σ9 GB; (d) Σ11 GB; (e) Σ13 GB. Panels (a1)–(e1) represent the GB structures before energy minimization and panels (a2)–(e2) represent the GB structures after relaxation and quenching.

In this work, five STGBs are considered and the parameters are listed in Table 1. These GBs are high angle GBs based on the 15° Brandon criterion. The STGBs were observed with a concentration higher than that of random GBs according to the experiments.[52,53] In our calculations, the GB energy ranges from 963 mJ·m^{-2} to 1467 mJ·m^{-2}, as shown in Table 1, which is consistent with other works.[55] For example, Vasily *et al.*[55] studied the GB energy for FCC metals recently. Their results pointed out that the random GB energy is about 1.445±0.032 J·m^{-2} in Ni bulk. The experiments showed that the concentration of $\Sigma3(112)$STGB is >10 multiples of a random distribution (MRD) of GBs.[52,54] In our calculations, the $\Sigma3(1\bar{1}2)[110]$ GB has the lowest GB energy (963 mJ·m^{-2}). The initial and final stable STGB structures are both shown in Fig. 1, in which the blue balls represent the FCC crystal structure, the red balls represent the irregular crystal structure, and the green balls represent the HCP crystal structure. The partial sections of the GB planes are inserted in the right of the full GB structures, which present the final stable GB structures after relaxation and quenching. Due to the periodic boundary conditions applied in all directions, the GB plane slightly slides when the energy minimization using the CG algorithm is carried out. However, the final GB structure is still much more stable, which can be used to finish the study of He doping behavior.

Table 1. Simulation parameters, including Σ (the reciprocal density of coincidence sites of two interpenetrating lattices misoriented by a relative rotation), the grain boundary (GB) plane (normal to the *z*-direction), 0° GB plane (*XY*), rotation axis [*X*], the disorientation angle θ about the corresponding tilt axis (*x*-direction), the GB energy, the simulation cell size, and the number of atoms.

Σ and GB plane	0° GB plane (*XY*)	Rotation axis [*X*]	θ/(°)	GB energy /mJ·m^{-2}	*x*/Å	*y*/Å	*z*/Å	Number of atoms
$\Sigma3(1\bar{1}2)$	[001]	[110]	70.52	963	64.76	61.01	109.30	41600
$\Sigma5(0\bar{2}1)$	[001]	[100]	126.80	1467	63.28	62.89	100.62	36864
$\Sigma9(1\bar{1}4)$	[001]	[110]	38.94	1268	64.94	63.58	106.57	39936
$\Sigma11(332)$	[110]	[1$\bar{1}$0]	50.47	1166	74.79	70.16	117.26	56160
$\Sigma13(0\bar{3}2)$	[001]	[100]	112.60	1355	63.53	63.63	117.47	43200

Generally, the GB configurations will significantly influence the thermal stability of the GB, the preferential GB segregation site for defects, and the segregation energy of solutes. The most stable GB configurations can be obtained by the process of energy minimization. In this work, the GB energy, γ_{gb}, is calculated by

$$\gamma_{gb} = \frac{E(\mathrm{GB}) - E(\mathrm{bulk})}{2S}, \tag{1}$$

where $E(\mathrm{GB})$ is the total energy of the simulation cell that contains GBs, $E(\mathrm{bulk})$ is the total energy of a Ni crystal composed of the same number of atoms, and S is the area of the GB plane in the simulation cell.

The formation energy of the He_N defect within the GB is determined by comparing the total energy of a GB containing the defect to the energy of the GB without the defect. The formation energy of the He_N defect within the GB, $E_\mathrm{f}(\mathrm{He}_N^{\mathrm{GB}})$, is given by

$$E_\mathrm{f}(\mathrm{He}_N^{\mathrm{GB}}) = E_\mathrm{tot}(\mathrm{GB} + \mathrm{He}_N) - E_\mathrm{tot}(\mathrm{GB}), \tag{2}$$

where $E_\mathrm{tot}(\mathrm{GB} + \mathrm{He}_N)$ is the total energy of the GB that contains the He_N defect after relaxation, and $E_\mathrm{tot}(\mathrm{GB})$ is the total energy of the grain without the defect. The cohesive energy of a perfect He crystal is negative and very small, so it is not included in Eq. (2).

The interaction strength of the He_N defect to a GB is evaluated by the binding energy. Two types are considered here: (I) the binding energy of the N-th He atom to the remaining He_{N-1} defect in a GB, e.g., $E_\mathrm{b}^{\mathrm{He}_{N\mathrm{th}}^{\mathrm{GB}} \to \mathrm{He}_{N-1}^{\mathrm{GB}}}$ in Eq. (3), (II) the binding energy of the He_N defect to the GB, e.g., $E_\mathrm{b}^{\mathrm{He}_N^{\mathrm{GB}} \to \mathrm{GB}}$ in Eq. (4).

In this work, the binding energy of the N-th He atom to the remaining He_{N-1} defect in a GB, $E_\mathrm{b}^{\mathrm{GB}}(\mathrm{He})$, is defined as

$$E_\mathrm{b}^{\mathrm{GB}}(\mathrm{He}) = E_\mathrm{f}(\mathrm{He}_{N-1}) + E_\mathrm{f}(\mathrm{He}) - E_\mathrm{f}(\mathrm{He}_N), \tag{3}$$

where E_f is the corresponding formation energy.

The total binding energy of the He_N defect interacting with the GB can be obtained by comparing the formation energy of the He_N defect in Ni bulk to that in the GB. Here, the binding energy of the He_N defect to the GB, $E_\mathrm{b}^{\mathrm{GB}}(\mathrm{He}_N)$, is calculated by

$$E_\mathrm{b}^{\mathrm{GB}}(\mathrm{He}_N) = E_\mathrm{f}^{\mathrm{bulk}}(\mathrm{He}_N) - E_\mathrm{f}^{\mathrm{GB}}(\mathrm{He}_N), \tag{4}$$

where $E_\mathrm{f}^{\mathrm{bulk}}(\mathrm{He}_N)$ is the formation energy of the He_N defect in Ni bulk, which is calculated by equation $E_\mathrm{f}(\mathrm{He}_N) = E_\mathrm{tot}(\mathrm{He}_N) - N\varepsilon_{\mathrm{He}} - L\varepsilon_{\mathrm{Ni}}$, where $E_\mathrm{tot}(\mathrm{He}_N)$ is the total energy containing He_N cluster in Ni bulk, $\varepsilon_{\mathrm{He}} = (-0.0071\ \mathrm{eV})$ is the cohesive energy of a He crystal, and $\varepsilon_{\mathrm{Ni}} = (4.4447\ \mathrm{eV})$ is the cohesive energy of a Ni crystal. The binding energy of the N-th He atom to the remaining He_{N-1} defect is obtained by equation $E_\mathrm{b}(\mathrm{He}) = E_\mathrm{f}(\mathrm{He}_{N-1}) + E_\mathrm{f}(\mathrm{He}) - E_\mathrm{f}(\mathrm{He}_N)$, where the formation energy of an interstitial He atom in Ni bulk is $E_\mathrm{f}(\mathrm{He}) = 4.06$ eV, which is very consistent with the results

of Mizuno *et al.*[56] and Meliu *et al.*,[57] and $E_f(He_N)$ is the formation energy of the He_N defect in Ni bulk. In Eq. (4), $E_f^{bulk}(He_N)$ is the formation energy of the He_N defect in Ni bulk, and $E_f^{GB}(He_N)$ is the formation energy of the He_N defect in the GB. Generally, a positive binding energy means that it is energetically favorable for the He_N defect to segregate into the GB, while a negative binding energy means that the defect does not prefer to segregate into the GB.

Table 2. The formations energy E_f and binding energy E_b of He_N clusters in Ni bulk (in units of eV).

He_N cluster	He_2	He_3	He_4	He_5	He_6	He_7	He_8	He_9	He_{10}
E_f	7.96	11.32	14.65	17.78	19.96	22.87	25.75	28.46	30.47
E_b	0.32	0.78	0.81	1.01	1.96	1.23	1.26	1.43	2.13

3. Results and discussion

Helium embrittlement in Ni-based alloys is a common issue, which can be controlled to a significant degree by controlling the diffusion and segregation of He defects in Ni bulk and in GBs. In this work, a set of model GBs are explored to provide insight into the role of structure in the He segregation behavior at GBs, while the real material has a much wider range of GB properties. To complete the binding energy calculation of an interstitial He atom in the GB, we first plot the formation energy of the He defect in various GB sites against its distance from the planes to quantify the change of the formation energy. Figure 2 is an example of such a plot for five STGBs. In this plot, the formation energy (Eq. (2)) minimizes near the GB planes, which is consistent with other works.[28,58–60] For example, Tschopp *et al.*[28] studied the binding energy of interstitial He and di-He defects to the GB structures in α-Fe. They pointed out that in the GB planes, the formation energy of one He atom and two He atoms is the minimum. The formation energy of an interstitial He atom is 2.30 eV in the $\Sigma3$ GB plane and is the lowest among the five STGBs, which suggests that it is easier for an interstitial He atom to segregate into the $\Sigma3$ GB plane. In $\Sigma5$, $\Sigma9$, $\Sigma11$, and $\Sigma13$ GB planes, the formation energy of the He defect is 3.05 eV, 2.28 eV, 3.40 eV, and 3.28 eV, respectively, among which the formation energy is highest for $\Sigma11$ GB. By comparing the formation energy of an interstitial He defect in Ni bulk ($E_f^{Ni+He} = 4.06$ eV) to that ($E_f^{GB+He} = 2.28$–3.40 eV) in the GB planes, we find that it is easier for the He defect to segregate into the GB planes. Our results can provide important insights to explain why He bubbles tend to segregate into the GB planes. The characteristic length of He defect segregation is studied only within 8.0 Å. In the far away region from the GB plane, the formation energy will be nearly 4.06 eV, which is equal to that in the Ni bulk environment. The main GB-affected region is shaded (light yellow) in Fig. 2. Except for $\Sigma9$, the distribution of the formation energy of the helium defect in GBs demonstrates certain symmetry around the GB planes, highlighting the symmetric nature of these GB configurations. Actually, after the relaxation and quenching process, the central position of the $\Sigma9$ GB plane exhibits a large shift relative to the initial position, which can be used to explain why the formation energy of an interstitial He atom around the $\Sigma9$ GB plane does not show the symmetry as that around other GB planes.

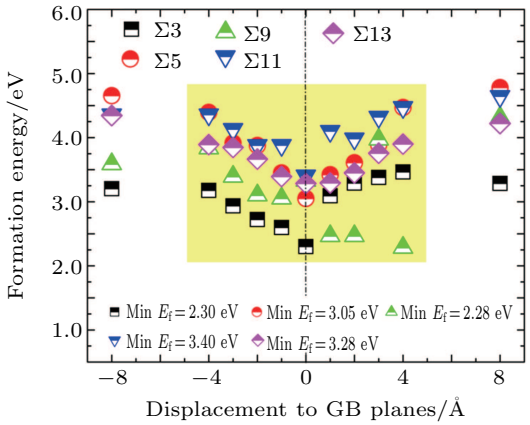


Fig. 2. (color online) The formation energy of an interstitial helium defect in the GB as a function of the initial distance of the He atom to the GB plane. The shaded area indicates the main interaction region.

Based on the formation energy calculations, the binding energy of an interstitial helium defect to various GBs as a function of its distance to the GB planes is explored. From Fig. 3, we can see that the binding energy reaches a maximum when an interstitial He defect locates at the GB planes. Some binding energy turns out to be negative, suggesting that the He defect does not like to stay at those positions. The $\Sigma3$ GB having a much lower GB energy possesses the highest binding energy of an interstitial He defect (Max $E_b = 1.84$ eV). For all GB structures, there is a largest binding energy in the GB plane, as shown in Fig. 3. Our results are consistent with other works.[28,54] For example, Tschopp *et al.*[54] studied the binding energy of He_NV_1 defects to α-Fe GBs. Their results showed that the $\Sigma3(112)$ "twin" GB has significantly lower binding energy for all He_NV_1 defects than other GBs, which are very consistent with our calculation.[54] Also notice that the $\Sigma3$ GB has the lowest GB energy, which explains its difference in the binding strength. For example, the study of He defects in the GB of α-Fe showed that the formation energy (and consequently, binding energy) for each particular GB is related to the GB energy.[28,54]

To understand the effect of GB characteristics on He_N defect absorption, we investigate the binding energy of an interstitial He defect to the GB plane against the disorienta-

tion angle and the GB energy, respectively. Figure 4 plots the relationship between the binding energy of an interstitial He defect to the GB plane and the GB energy in the [001], [110], and [1$\bar{1}$0] tilt orientations. The GB energy ranges from 963 mJ·m^{-2} to 1583 mJ·m^{-2}. The $\Sigma3(1\bar{1}2)[110]$ GB with the lowest GB energy gives the highest binding energy. This suggests that the He$_N$ defect is easier to segregate into the GB having lower GB energy. For all other GBs, the binding energy of an interstitial He defect to the GB planes has slight difference as a function of the GB energy. For example, Tschopp *et al.*[60] pointed out that most GBs within the same tilt system ([001], [110], and [1$\bar{1}$0]) have very similar binding energy aside from a few "special" boundaries (e.g., the $\Sigma5\{310\}$, $\Sigma5\{210\}$, and $\Sigma3\{112\}$ STGBs) that have binding energy higher than that of the rest. Besides, for the [110] tilt orientation, as the GB energy increases, the binding energy decreases. However, for the [001] tilt orientation, the binging energy increases with the GB energy increasing.

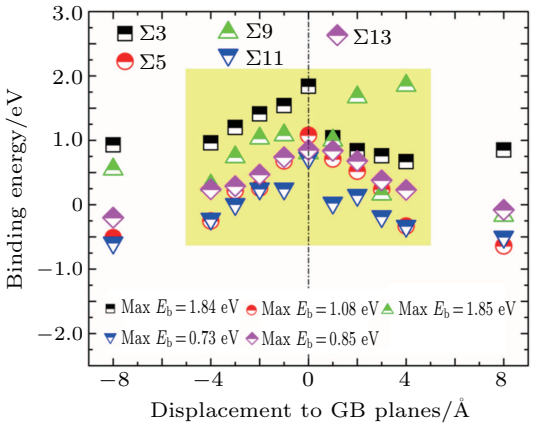


Fig. 3. (color online) The binding energy of an interstitial He atom to the GB plane as a function of the initial distance of the He atom to the GB plane. The shaded area indicates the main interaction region.

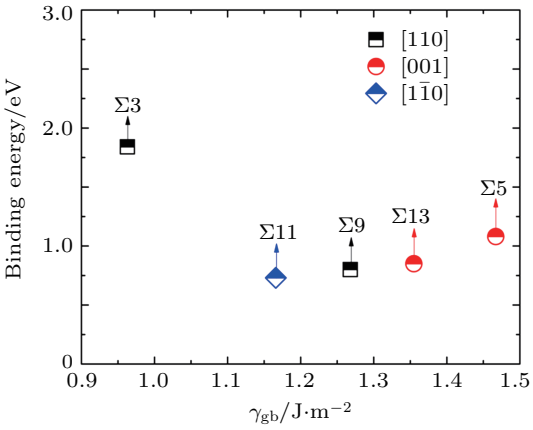


Fig. 4. (color online) The binding energy of an interstitial He defect to the GB plane for various GB configurations as a function of the GB energy.

We investigate the interaction between the He$_N$ defect and the GB plane by adding interstitial He atoms into the GB plane. Here, we first select ten random numbers to generate the initial configurations of the He$_N$ defect, and then obtain the stable configurations through the relaxation and quenching of the simulation system. From these stable He$_N$ defect configurations, the most stable state is chosen to analyze the binding energy. It should be noted that as the number of He atoms increases, the lattice Ni atoms will be kicked out, forming the self-interstitial Ni atoms. However, we only consider in this study the trapping strength of the He$_N$ defect in Ni bulk and at the GB: the self-interstitial generated Ni atom is ignored here. After the relaxation of the whole simulation system, the He$_N$ defect is kept at the position of the GB plane. The binding energy of an interstitial He defect to the remaining He$_{N-1}$ defect in the GB plane is calculated using Eq. (3). The dependence of the binding energy on the defect size is depicted in Fig. 5. With increasing the number of He atoms in the He$_N$ defect in the GB plane, the binding energy tends to increase. This suggests that the supplemental He atom bonds to the remaining He$_{N-1}$ defect and it tends to grow to decrease the total energy of the simulated system, which is very consistent with the experimental results.[61] The binding energy of the He defect to the remaining He$_{N-1}$ defect is positive in the GB planes, except for $\Sigma5$ and $\Sigma11$ GBs with negative values when the number of He atoms is 6. The negative binding energy indicates that the He atoms occupy the plane positions but do not bind to each other. By comparing the binding energy of an interstitial He defect to the remaining He$_{N-1}$ defect in Ni bulk and that in the GB plane, we find that the majority of the binding energy is generally higher in Ni bulk than that in the GB plane, which tells us that the He$_N$ defect is much more stable in Ni bulk than in the GB plane environment. Besides, there is some maximum value as the number of He defects increases. For example, the maximum binding energy of an interstitial He defect to the remaining He$_{N-1}$ defects is 2.34 eV for the $\Sigma11$ GB when the number of He atoms is seven. For the $\Sigma3$, $\Sigma5$, $\Sigma9$, and $\Sigma13$ GBs, the maximum binding energy of an interstitial He defect to the remaining He$_{N-1}$ defects is 1.52 eV, 1.74 eV, 1.86 eV, and 0.89 eV, respectively, which suggests that at this point, the He$_N$ defect is the most stable. The majority of the binding energy does not exceed 2.0 eV, which is consistent with other work.[18] These results suggest that the local GB environment has a significant impact on the stable structures of the He$_N$ defect as well as on their trapping strength in the GB plane.

On the basis of the discussion about the binding energy of an interstitial He to the remaining He defects, we further investigate the binding strength of the He$_N$ defect to the GB plane. All calculations are performed with Eq. (4). The binding energy of the He$_N$ defect to the GB plane is plotted as a function of the number of He atoms. In this plot, all the binding energies are positive, and the binding energy increases with the

He_N defect size, as shown in Fig. 6. Additionally, the binding energy of an interstitial He defect to the GB plane is 1.25 eV, 1.90 eV, 1.28 eV, 1.99 eV, and 1.98 eV, respectively, for the Σ3, Σ5, Σ9, Σ11, and Σ13 GBs. By comparing the binding energy of an interstitial He defect to a vacancy ($E_b^{HeV+Ni} = 2.44$ eV) in Ni bulk with that to the GB plane ($E_b^{He+GB} = 1.25$–1.99 eV), we find that the trapping strength of the GB plane to an interstitial He defect is weaker than that of the vacancy in Ni bulk, which is consistent with the results of binding strength of He and di-He defects to the Σ5(310)[001] GB plane in α-Fe.[34] These results can provide insights in understanding the He embrittlement or He damage in Ni-based alloys for future Generation-IV MSR.

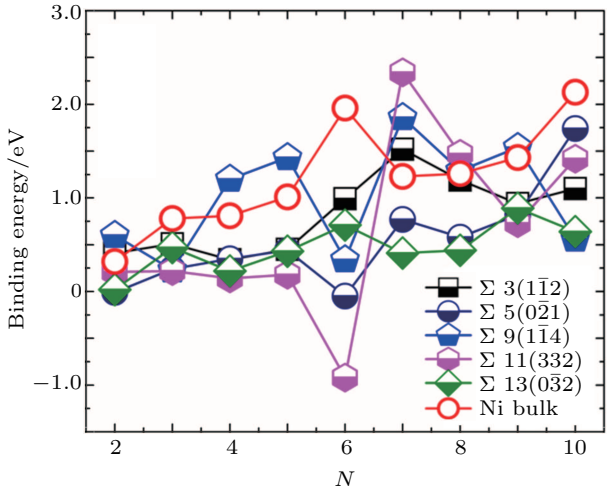


Fig. 5. (color online) The binding energy of the N-th He defect to the remaining He_{N-1} defect as a function of the number of He atoms in the defect.

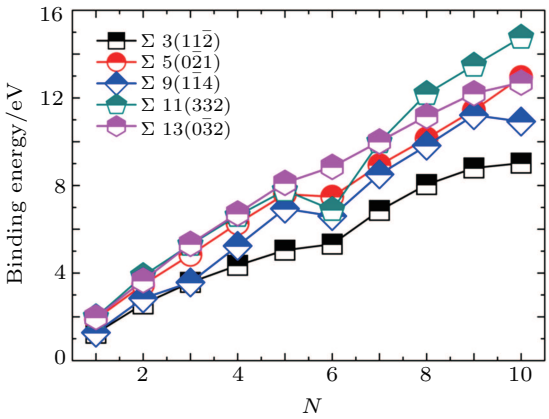


Fig. 6. (color online) The binding energy of the He_N defect to the GB plane as a function of the number of He atoms in the defect.

4. Conclusion

The interaction between the He_N defect and the GBs of Ni bulk was studied using MD simulations. Five high angle STGBs with [100], [110], and [1$\bar{1}$0] tilt orientations were investigated. We calculated the formation energy and the binding energy of an interstitial He defect in all potential GB sites within a length scale of 8.0 Å. The results show that the binding energy of an interstitial He defect to the GB plane is the strongest among all sites around the plane. The He_N defect is much more stable in Ni bulk than in the GB plane. In addition, the binding energy of an interstitial He defect to a vacancy is stronger than that to a GB plane. The binding strength between the GB and the He_N defect increases with the He_N defect size, and the binding strength of the He_N defect to the Σ3(1$\bar{1}$2)[110] GB is the weakest. This study is helpful to understand how a GB interacts with the He_N defect in a FCC crystal, how the GB configuration affects the He defect trapping mechanism, and ultimately how they affect the He (re-)combination and embrittlement in the GB for Ni-based alloys.

Acknowledgement

The Shanghai Supercomputing Center and Lanzhou Supercomputing Center are acknowledged for allocation of computing time.

References

[1] Zinkle S J 2005 *Phys. Plasmas* **12** 058101
[2] Ishiyama Y, Kodama M, Yokota N, Asano K, Kato T and Fukuya K 1996 *J. Nucl. Mater.* **239** 90
[3] Stoller R E and Odette G R 1988 *J. Nucl. Mater.* **155** 1328
[4] Lewis M B and Farrell K 1986 *Nucl. Instrum. Methods Phys. Res. B* **16** 163
[5] Bloom E E, Busby J T, Duty C E, Maziasz P J, McGreevy T E, Nelson B E, Pint B A, Tortorelli P F and Zinkle S J 2007 *J. Nucl. Mater.* **367** 1
[6] Zinkle S J and Busby J T 2009 *Mater. Today* **12** 12
[7] Yamamoto T, Odette G R and Kishimoto H 2006 *J. Nucl. Mater.* **356** 27
[8] Trinkaus H and Singh B N 2003 *J. Nucl. Mater.* **323** 229
[9] Johnson P B and Mazey D J 1978 *Nature* **276** 595
[10] Trinkaus H and Singh B N 2003 *J. Nucl. Mater.* **318** 234
[11] Zinkle S J and Busby J T 2009 *J. Nucl. Mater.* **386** 8
[12] Trinkaus H 1983 *Radiation Effects* **78** 189
[13] Kalashnikov A N, Chernov I I, Kalin B A and Binyukova S Y 2002 *J. Nucl. Mater.* **307** 362
[14] Edmondson P D, Parish C M, Zhang Y and Hallén A 2011 *Scripta Mater.* **65** 731
[15] Lane P L and Goodhew P J 1983 *Philos. Mag. A* **48** 965
[16] Lefaix-jeuland H, Moll S, Jourdan T and Legendre F 2013 *J. Nucl. Mater.* **434** 152
[17] Tschopp M A and McDowell D L 2007 *Philos. Mag.* **87** 3147
[18] Baskes M I and Vitek V 1985 *Metall. Trans. A* **16** 1625
[19] Yamaguchi M, Nishiyama Y and Kaburaki H 2007 *Phys. Rev. B.* **76** 0355418
[20] Wachowicz E and Kiejna A 2011 *Modell. Simul. Mater. Sci. Eng.* **9** 025001
[21] Rhodes N R, Tschopp M A and Solanki K N 2013 *Modell. Simul. Mater. Sci. Eng.* **21** 035009
[22] Kurtz R J and Heinisch H L 2004 *J. Nucl. Mater.* **329** 1199
[23] Gao F, Heinisch H L and Kurtz R J 2006 *J. Nucl. Mater.* **351** 133
[24] Kurtz R J, Heinisch H L and Gao F 2008 *J. Nucl. Mater.* **382** 134
[25] Gao F, Heinisch H L and Kurtz R J 2009 *J. Nucl. Mater.* **386** 390
[26] Zhang L, Shu X L, Jin S, Zhang Y and Lu G H 2010 *J. Phys.: Condens. Matter* **22** 375401
[27] Zhang L, Fu C C and Lu G H 2013 *Phys. Rev. B* **87** 134107
[28] Tschopp M A, Gao F, Yang L and Solanki K N 2014 *J. Appl. Phys.* **115** 1
[29] Xia J X, Hu W Y, Yang J Y and Ao B Y 2006 *Phys. Stat. Soli. B* **243** 1
[30] Terentyev D and He X 2010 *Comput. Mater. Sci.* **49** 858
[31] Hafez H S Z, Lucas G and Schäublin R 2009 *Europhys. Lett.* **85** 6008
[32] Demkowicz M J, Bhattacharyya D, Usov I, Wang Y Q, Nastasi M and Misra A 2010 *Appl. Phys. Lett.* **97** 161903

[33] Zhang Y F, Millett P C, Tonks M and Zhang L Z 2012 *J. Phys.: Condens. Matter* **24** 305005
[34] Zhang L, Zhang Y and Lu G H 2013 *J. Phys.: Condens. Matter* **25** 095001
[35] Hammond K D, Hu L, Maroudas D and Wirth B D 2015 *Europhys. Lett.* **110** 52002
[36] Kashinath A, Misra A and Demkowicz M J 2013 *Phys. Rev. Lett.* **110** 086101
[37] http://lammps.sandia.gov/
[38] Daw M S and Baskes M I 1984 *Phys. Rev. B* **29** 6443
[39] Baskes M I 1992 *Phys. Rev. B* **46** 2727
[40] Ouyang Y, Zhang B, Liao S and Jin Z 1996 *Phys. B* **101** 161
[41] Deng H, Hu W, Shu X and Zhang B 2003 *Surf. Sci.* **543** 97
[42] Yang J, Hu W, Deng H and Zhao D 2004 *Surf. Sci.* **572** 2074
[43] Hu W, Zhang B, Huang B, Gao F and Bacon D J 2001 *J. Phys.: Conden. Matter* **13** 1193
[44] Hu W, Deng H, Yuan X and Fukumoto M 2003 *Euro. Phys. J. B* **34** 429
[45] Hu W, Shu X and Zhang B 2002 *Comput. Mater. Sci.* **23** 175
[46] Hu W and Fukumoto M 2002 *Modell. Simula. Mater. Sci.* **10** 707
[47] Johnson R A 1990 *Phys. Rev. B* **41** 9717
[48] Baskes M I and Melius C F 1979 *Phys. Rev. B* **20** 3197
[49] Johnson R A 1973 *J. Phys. F: Metal Phys.* **3** 295
[50] Nosé S 1991 *Prog. Theor. Phys. Suppl.* **103** 1
[51] https://staff.aist.go.jp/h.ogawa/GBstudio/indexE.html
[52] Beladi H and Rohrer G S 2013 *Acta Mater.* **61** 1404
[53] Beladi H and Tphrer G S 2013 *Metall. Mater.Trans. A* **44** 115
[54] Tschopp M A, Gao F and Solanki K N 2014 *J. Appl. Phys.* **115** 1
[55] Bulatov V V, Reed B W and Kumar M 2014 *Acta Mater.* **65** 161
[56] Mizuno T, Asato M, Hoshino T and Kawakami K 2001 *J. Magn. Magn. Mater.* **226** 386
[57] Baskes M I and Melius C F 1981 *Phys. Rev. B* **20** 3197
[58] Demkowicz M J, Anderoglu O, Zhang X and Misra A 2011 *J. Mater. Res.* **26** 1666
[59] Bai X M, Vernon L J, Hoagland R G, Voter A F, Nastasi M and Uberuaga B P 2012 *Phys. Rev. B* **85** 214103
[60] Tschopp M A, Solanki K N, Gao F, Sun X, Khaleel M A and Horstemeyer M F 2012 *Phy. Rev. B* **85** 064108
[61] Ryazanov A, Voskoboinikov R E and Trinkaus H 1996 *J. Nucl. Mater.* **1085** 233